Pergamon

PII: S1359-6454(96)00332-1

Acta mater. Vol. 45, No. 5, pp. 1931–1940, 1997

1359-6454/97 $17.00 + 0.00

PRESSURE INFLUENCE ON THE GRAIN BOUNDARY WETTING PHASE TRANSITION IN Fe–Si ALLOYS

B. STRAUMAL[1,2], E RABKIN[1], W. ŁOJKOWSKI[3], W. GUST[1] and L. S. SHVINDLERMAN[2]

[1]Max-Planck-Institut für Metallforschung and Institut für Metallkunde, Seestr. 75, D-70174 Stuttgart, Germany, [2]Institute of Solid State Physics, Russian Academy of Sciences, Chernogolovka, 142432 Russia and [3]High Pressure Research Centre, Polish Academy of Sciences, Sokolowska 29, 01 142 Warsaw, Poland

(Received 15 January 1996; accepted 21 August 1996)

Abstract—The influence of hydrostatic pressure up to 1.4 GPa at 905°C on the wetting of grain boundaries in Fe–6 at.% Si and Fe–12 at.% Si bicrystals by a Zn-rich melt has been studied. The dihedral angle θ at the intersection of the grain boundary with the solid/liquid interface has been measured by light microscopy. The transition from complete ($\theta = 0$) to partial ($\theta > 0$) wetting of the grain boundary (dewetting phase transition) was found to occur as the pressure increased. The dewetting transition pressure is higher for special boundaries than for the general boundary studied and decreases with increase in the Si content in the alloy. The pressure effect on the solidus concentration of Zn in Fe–Si alloys has been determined. This enabled us to construct the surfaces of grain boundary wetting/dewetting phase transitions in three-dimensional phase diagrams in Zn concentration–temperature–pressure and Zn concentration–Si concentration–pressure coordinates. A thermodynamic analysis of the wetting phenomena in binary and ternary systems is given, taking into account the effect of pressure, chemical interactions and structural misfit on the energy of interfaces. © *1997 Acta Metallurgica Inc.*

1. INTRODUCTION

High pressures play an important role in many technological processes involving wetting phenomena: soldering, brazing, liquid phase assisted sintering, etc. However, only very limited information about the influence of high pressures on the wetting of metal surfaces is available. This is due to the difficulties connected with the oxidation of free surfaces and with the strong influence of the gases adsorbed on their energetic characteristics [1]. In this respect experiments on the wetting of internal interfaces in solids have an important advantage compared to classical wetting experiments with the sessile drop: the interfaces that determine the wetting behaviour are "hidden" inside the sample and the influence of the pressure agent on the properties of interfaces can be avoided. On the other hand, when the grain boundary (GB) wetting is considered the GB crystallography must be taken into account, which increases the number of the degrees of freedom (DOF) of the system [2]. In the present experiments, from the eight DOF of the GB [2] only one was varied: the tilt angle ϕ of $\langle 001 \rangle$ symmetrical tilt boundaries in oriented bicrystals. Nevertheless, this new parameter considerably complicates the theoretical treatment of the problem in multi-component system, as is the case during wetting experiments. One of the reasons is that only few data exist about the misorientation dependence of the GB energy in alloys [3].

The equilibrium of a bicrystal in contact with a liquid metal can be characterized by the dihedral angle θ at the site of intersection of the GB and the solid/liquid interface (Fig. 1). The angle θ is defined by the condition of equilibrium:

$$\cos\left(\frac{\theta}{2}\right) = \frac{\gamma_{GB}}{2\gamma_{SL}} \tag{1}$$

where γ_{GB} and γ_{SL} are the excess free energies of the GB and solid/liquid interface, respectively, and the torque terms for the interfacial energies are neglected. The two situations $\theta > 0$ and $\theta = 0$ correspond to partial wetting and complete wetting, respectively. If some intensive thermodynamic variables like temperature, composition, pressure or the GB misorientation angle are altered, a transition from partial to complete wetting can occur. This is the wetting phase transition, which can be of first or second order [Fig. 1(b)]. For example, one can often observe the GB wetting phase transition as the temperature is increased or the misorientation angle is varied [4, 5]. When the situation is reversed and the temperature is decreased, the value of θ changes from zero to non-zero values. This is called the dewetting phase transition. The relation between the wetting transition temperature T_w, the transition pressure p_w, the composition and the misorientation angle is determined by the equation

$$\gamma_{GB}(T_w, p_w, \phi) = 2\gamma_{SL}(T_w, p_w, \phi). \tag{2}$$

The lines of the GB wetting/dewetting phase transitions in the traditional bulk phase diagrams play an important role in forming the microstructure of multiphase alloys in thermodynamic equilibrium [4]. At temperatures above the wetting phase transition temperature, T_w, the phase that wets the GBs completely should be present as a continuous layer along the GBs; at temperatures below T_w this phase is present in the form of isolated droplets on the GBs or inside the grains. Since γ_{SL} and γ_{GB} depend on the crystallographic parameters and chemical composition, the p_w and T_w values should depend on these parameters as well. There are few experimental data on the effect of the GB misorientation on T_w. In the Cu–In system the value of T_w for a symmetrical $\langle 011 \rangle$ tilt GB close to the symmetrical coherent twin boundary was only about 30°C higher than for the general 141°$\langle 011 \rangle$ GB, though the excess free energy difference for these GBs in pure Cu was about 50% [5]. In the Al–Sn system the value of T_w for a symmetrical 38.5°$\langle 011 \rangle$ tilt GB close to the Σ9 coincidence misorientation (Σ being the reciprocal density of the coincidence sites) was about 13°C higher than for the general 32°$\langle 011 \rangle$ GB, though almost in the whole temperature interval studied the relative value of γ_{GB} was higher for this special GB than for the general GB [4]. It is seen that the GB misorientation and energy influence the T_w value. However, the magnitude of the temperature change cannot be predicted in a straightforward manner.

As far as the pressure effect on the GB wetting is concerned, it was shown earlier [6] that the dewetting phase transition resulting from an increase in the pressure occurs in Fe–6 at.% Si bicrystals in the pressure range 0.2–0.6 GPa and in the temperature interval 700–900°C. It was also shown that the temperature dependence of p_w correlates with the temperature dependence of the solubility of Zn in Fe: the maximal solubility at the peritectic temperature of 790°C corresponded to the minimal p_w value [6]. The aim of the present paper was to investigate the dependence of the dewetting transition pressure p_w on the macroscopical DOF of GBs and the composition of the alloy.

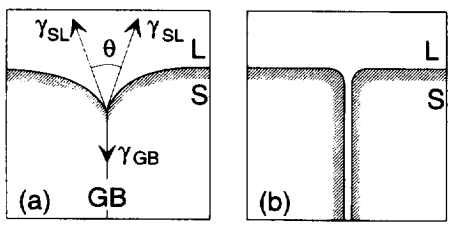

Fig. 1. Schematic showing partial (a) and complete (b) wetting of a GB by a melt; γ_{GB} and γ_{SL} are the excess free energies of the GB and solid/liquid interface, respectively. L and S are the solid and liquid phases, respectively.

2. EXPERIMENTAL

2.1. Preparation of the bicrystals

The Fe–Si alloys containing 6 and 12 at.% Si were prepared from Si of 99.999 wt % purity and Fe of 99.99 wt % purity. The single crystals of these alloys were grown in vacuum by electron beam floating zone melting. To prepare oriented single crystalline seeds, a crystallographically perfect single crystal was grown and cut to obtain cylindrical pieces 15–20 mm in length and 12–15 mm in diameter. Two parallel surfaces of a seed were checked carefully by X-ray diffraction with an accuracy of about 1° and then polished in order to make very clean and mirror-like surfaces. Before growing, the lower holder with a seed on the top of it, a cylindrical ingot and an upper holder are joined together by *in situ* local electron beam welding of the contacting surfaces. The seeding procedure consists of melting a narrow liquid zone in the seed just under the seed/ingot interface. After an initial liquid zone is created, the electron gun is moved up vertically together with the liquid zone until the whole specimen becomes single crystalline.

In principle, the growing procedure for Fe–Si bicrystals is similar to that for single crystals. The bicrystalline seeds need a similar careful preparation to that for single-crystalline seeds but because they are made up of two half-cylinders, the quality of the interface between them is of great importance. They had to be carefully ground, etched and polished to obtain the clean and flat surfaces to be joined together. The bicrystalline seeds are composed using two single-crystalline halves. The misorientation angle ϕ of a tilt GB is formed by oriented cutting of single crystals. The Fe–6 at.% Si bicrystal with a symmetrical $\langle 001 \rangle$ tilt GB and a misorientation angle $\phi = 43°$ was grown in this, with the misorientation close to the Σ29 coincidence GB misorientation (43.6°); however, according to the classification proposed earlier [7], at temperatures above 0.5 T_m this GB should not demonstrate any special properties (here T_m is the melting temperature). Two other bicrystals with misorientation angles of 35° (2° deviation from the 36.9° coincidence Σ5 misorientation) and 38° (1° deviation from the Σ5 GB) were grown from bicrystalline seeds obtained after cutting "piece of cake" segments from the 43°$\langle 001 \rangle$ bicrystal and putting two monocrystalline parts together. The misorientation angles of the grown bicrystals were then checked again by X-ray diffraction and by the etching pits observed in the optical microscope. The undesirable twist and second tilt components of the misorientation angle were below 1.5° for all bicrystals obtained.

Figure 2 shows the scheme for sample cutting and preparation of the specimens used for the GB wetting studies. First, the seeds were removed by spark erosion. Only the 30–40 mm long part of the bicrystals close to the seeds were used for further investigations. These parts of the bicrystals were then

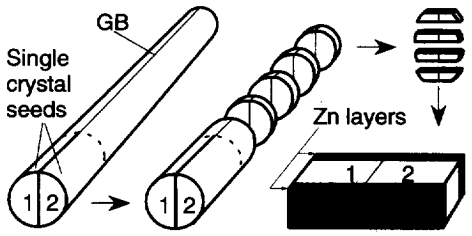

Fig. 2. Schematic of sample cutting for wetting experiments.

cut perpendicular to the growth axis in about 2 m thick slices. The elongated samples were than cut from these slices in such a way that the GB was in the middle of the long dimension of each sample and perpendicular to it (see Fig. 2). These samples were carefully polished on a 4000 grit SiC paper and chemically polished in a solution of 80 ml H_2O_2, 14 ml H_2O and 6 ml HF. A 100–200 μm thick Zn layer was applied to the surface of each sample by immersing the specimen in a melt of Zn of 99.999 wt % purity at about 500°C. Then the Zn layer was partially removed from the two opposite sides of the bicrystal. Therefore, only two (001) surfaces of the bicrystal remained coated with Zn. Samples prepared by this method were then wrapped up into a Ta foil separately from each other and placed into a stainless steel capsule (outer diameter 9.8 mm, inner diameter 7.9 mm). In the wall of the bottom part of the capsule a hole for a temperature sensor was drilled parallel to the capsule axis. Nearly 50 mm^3 of zinc were placed in the same bottom part of the capsule in order to prevent zinc evaporation from the sample surface during annealing.

2.2. *The high pressure annealing*

The capsule with the bicrystals in it was placed in a furnace that was fixed inside the high pressure cell made by the High Pressure Research Centre in Warsaw. The inner diameter of the high pressure cell, the inner diameter of the furnace tube and the length of the furnace were 30 mm, 10 mm and 200 mm, respectively. A temperature controller kept the temperature variations during the experiment at a level less than 1°C. The differences between readings on the thermocouples along the crucible were less than 2°C. Taking into account the low thermal capacity of the small furnace, a temperature controller with low time constants had to be used. The presence of condensed argon gas facilitated the heat transfer in the high pressure furnace. A good thermal contact between the thermocouples and the crucibles as well as the crucible and the furnace was assured if the lowest annealing pressure was at least 10 MPa. The heating time from 600°C to 905°C was 5 min. After annealing at 905°C for times varying from 2 h at low pressures to 5 h at high pressures (the annealing times are shown explicitly in Fig. 3), the specimens were quenched to room temperature. The thermocouple readings were corrected for the pressure effect using the correction terms of Cheng *et al.* [8]. The pressure in the high pressure unit was regulated with an accuracy of ± 5 MPa in the pressure range up to 400 MPa. Above 400 MPa the pressure was measured with an accuracy of 1% using a manganin gauge. The low time constants of the high

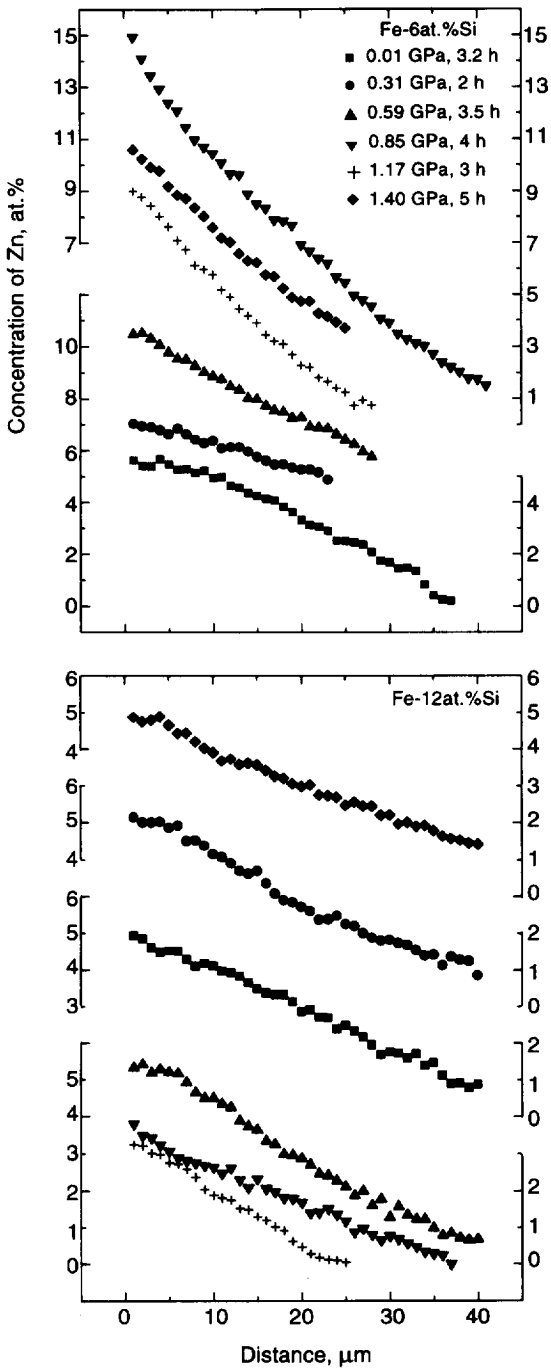

Fig. 3. Zn distribution in Fe–Si bicrystals near the surface after anneals under high pressures at 905°C. The interpolated Zn concentration at the "solidified Zn-rich alloy/Fe(Si) bicrystal" interface (0 μm), c_S^{Zn}, is accepted as the Zn solidus concentration. The solidus concentrations are maximal at pressures of 0.85 and 0.59 GPa for Fe–6 at.% Si and Fe–12 at.% Si, respectively.

pressure furnaces enabled cooling times of the order of 100 s. It has been shown [6] that the formation time for the GB groove at the temperature of the present experiment is about 2 ks. Therefore, the dihedral angle could not change in a measurable way during cooling of specimens to room temperature.

2.3. *Measurement of θ and Zn solidus concentration*

After the anneal the specimens were fixed in a holder by Wood's alloy and then mechanically ground and polished. On these specimens the dihedral angle θ at the GB was measured by light microscopy. Electron probe microanalysis (EPMA) measurements of the Zn concentration in the bicrystals after annealing were carried out on a JEOL 6400 electron probe microanalyser operated at 15 kV. The intensity of the ZnK_α peak was determined, and from it the Zn concentrations were obtained using a standard program for quantitative EPMA analysis.

An important question for such experiments is whether or not the dihedral angle θ measured on the optical micrographs with a spatial resolution of about 0.5 μm coincides with the true value of the dihedral angle on the microscopic scale. For example, a Bi-rich phase is present in ZnO varistor ceramics in the form of isolated inclusions at the GB triple junctions and macroscopically $\theta > 0$ at the contact point with the GB (partial wetting) [9]. However, transmission electron microscopy with a higher magnification reveals a continuous Bi-rich wetting film on the GB (complete wetting). The reason for such behaviour is the decrease in the excess energy of crystal/melt interfaces due to their interaction at short distances. In our case such a microscopic wetting layer of the Zn-rich phase at the GB would manifest itself in an enhanced GB diffusivity in the GB region adjacent to the liquid metal groove [10, 11]. However, we have conducted EPMA measurements of the GB diffusivity on some specimens annealed under hydrostatic pressure at which according to the observations on the optical micrographs the partial wetting of the GB by the Zn-rich phase occurs ($\theta > 0$). An enhanced GB diffusivity has not been found. Therefore, if $\theta > 0$ on the optical micrograph one can be sure that there is incomplete wetting of the GB on the microscopic scale, too.

3. RESULTS

The Zn distribution in the Fe–Si bicrystals near the surface after the diffusion anneals is shown in Fig. 3. Because the liquid Zn was present in the capsules during anneals at high pressure, the Zn concentration at the surface of the Fe–Si sample should correspond to the equilibrium solidus concentration. To determine this concentration, we have interpolated the measured concentration–distance dependencies by a three-degree polynomial and accepted the interpolated value at zero distance as the solidus concentration c_S^{Zn}; c_S^{Zn} demonstrates a maximum at 0.85 and 0.59 GPa for Fe–6 at.% Si and Fe–12 at.% Si, respectively.

Figure 4 shows optical micrographs of the site of intersection of the GB with the solid/liquid interface for different pressures. After slight etching for a few seconds in a solution of 70 ml H_2O and 30 ml HNO_3 the product of the solidification of the Zn-rich liquid phase is dark and the position of the crystal/melt interface can be clearly seen. The Zn-enriched diffusion zone can also be recognized in some bicrystals by the dark contrast. The GBs lie perpendicular to the position of the former crystal/melt interface and to the cross-section surface. This makes the measurements of the contact angle θ easier than in experiments on polycrystals where the droplets of a liquid phase are distributed randomly and the GBs are inclined to the cross-section surface. As shown in Fig. 4, the complete wetting of GBs by the Zn-rich melt occurs in all samples up to some pressure p_w, and for pressure above p_w the angle θ increases with increasing pressure (partial wetting). Therefore, one can conclude that at the pressure p_w the dewetting phase transition occurs on the GBs; p_w depends on the GB misorientation angle and on the Si content in the alloy. This is summarized in Fig. 5 where the pressure dependencies of the contact angle θ are shown. The pressure p_w is determined by extrapolation of the $\theta(p)$ dependence for $\theta > 0$ to $\theta = 0$. The error in the determination of p_w is therefore half the pressure interval where the transition occurs, except for the 43°⟨001⟩ GB in Fe–6 at.% Si where the error is higher.

The obtained experimental data are summarized in three-dimensional phase diagrams with the surfaces of the 38°⟨001⟩ GB wetting/dewetting phase transition in Zn concentration–temperature–pressure (Fig. 6) and Zn concentration–Si concentration–pressure (Fig. 7) coordinates. The data for the Zn solubility limit in Fe–12 at.% Si at the normal pressure of saturated Zn vapour are taken from previous work [11]. The surface of the GB phase transition for the Fe–12 at.% Si alloy in Fig. 6 is tilted with respect to the pressure axis because the wetting phase transition has been observed already at the normal pressure at 750°C [11]. This surface divides the two-phase area of the bulk phase diagram into two subspaces where complete wetting (low p, high T) and partial wetting (high p, low T) of the GB by the Zn-rich melt occur. In contrast to Fig. 6, the GB phase transition surface is only slightly tilted with respect to the Si concentration axis in Fig. 7 because the difference between the p_w values for the alloys with 6 and 12 at.% Si is only about 0.2 GPa.

The dependence of the dewetting phase transition pressure in Fe–6 at.% Si on the deviation from the Σ5 coincidence misorientation ($\phi = 36.9°$) is shown in Fig. 8. The shadowed area in this figure denotes the region of misorientations in which the GBs have a special structure and properties, characteristic of the Σ5 GB. This region was established earlier, based on

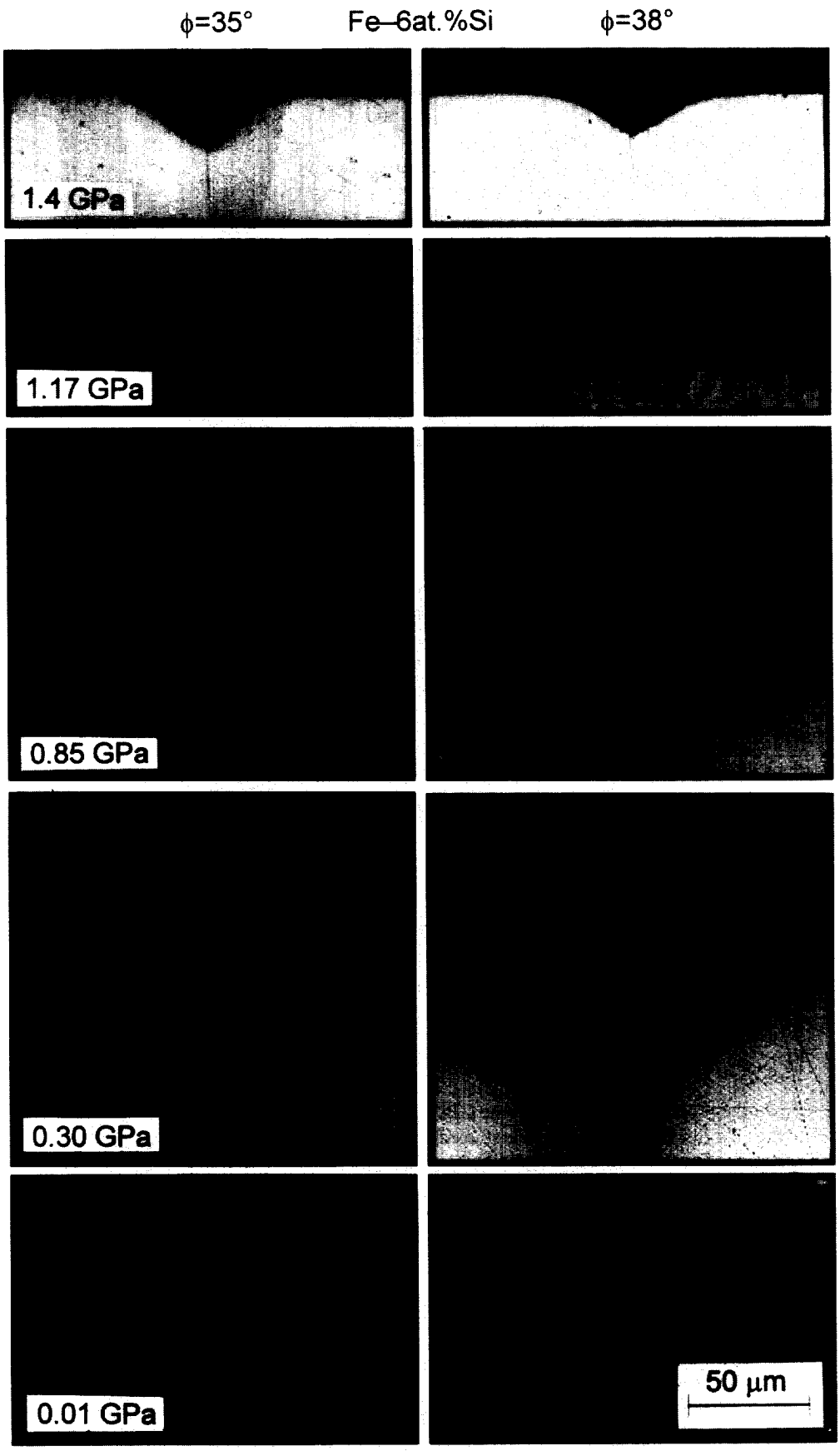

Fig. 4. Optical micrographs of contact areas between Fe(Si) bicrystals (below, bright) and Zn-rich melts (above, dark) after anneals at 905°C under different pressures.

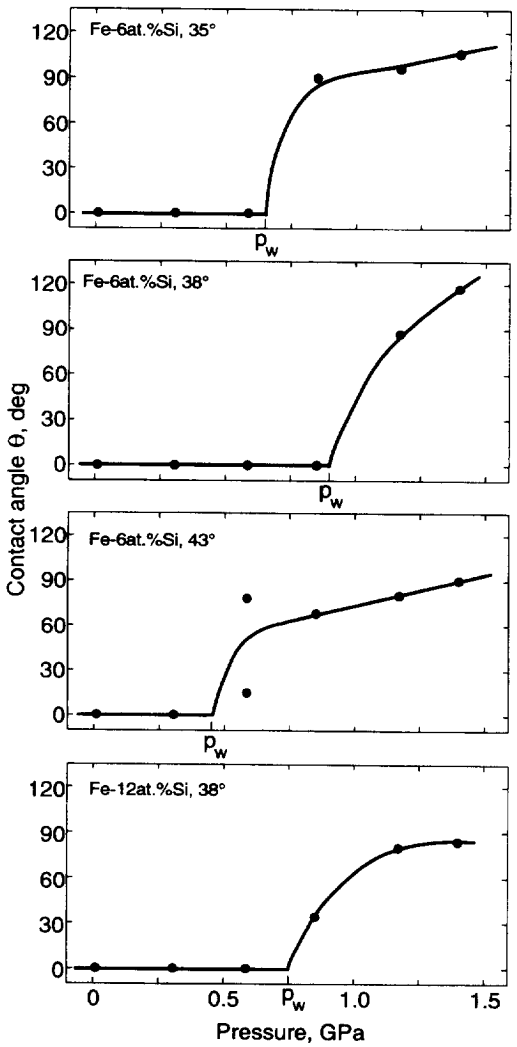

Fig. 5. Pressure dependencies of contact angle θ for GBs studied. As the pressure increases, the dewetting transition from complete to partial wetting occurs at p_w.

the analysis of the literature data [7]. The p_w has a minimal value of 0.4 GPa for the 43°⟨001⟩ general GB.

4. DISCUSSION

The results of the present study show that the GBs are wetted by the Zn-rich melt in all bicrystals studied at normal pressure. Therefore, the GB has a higher energy than two solid/liquid interfaces separated by the liquid phase. Further, there is a pressure in the range 0.4–0.9 GPa where the dewetting transition takes place and the two solid/liquid interfaces merge to form a GB. It follows from the above that the energy of the two solid/liquid interfaces increases with increasing pressure more rapidly than the energy of the GB. We may consider the following reasons for the effect of pressure on the energy of the investigated interfaces:

(i) excess volume of the interfaces;
(ii) the change in the solute concentration in the interfaces caused by the pressure. The composition at the solid/liquid interface corresponds to the solidus concentration, which was shown to change substantially with pressure (see Fig. 3). This changes the value of γ because excess energies of all interfaces forming the GB groove depend on the concentration.

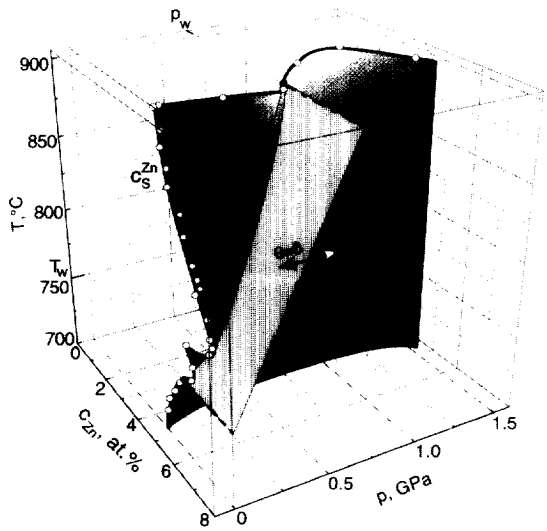

Fig. 6. Quasibinary three-dimensional bulk phase diagram for Fe–12 at.% Si–Zn system in Zn concentration–temperature–pressure coordinates along with surface of wetting/dewetting phase transition (light) for 38°⟨001⟩ tilt GB. The data on the solubility limit of Zn in the Fe–12 at.% Si alloy under normal pressure are taken from Ref. [11].

We think that the excess volume of interfaces is more important for the pressure dependence of their energy than the chemical effects. Indeed, if the

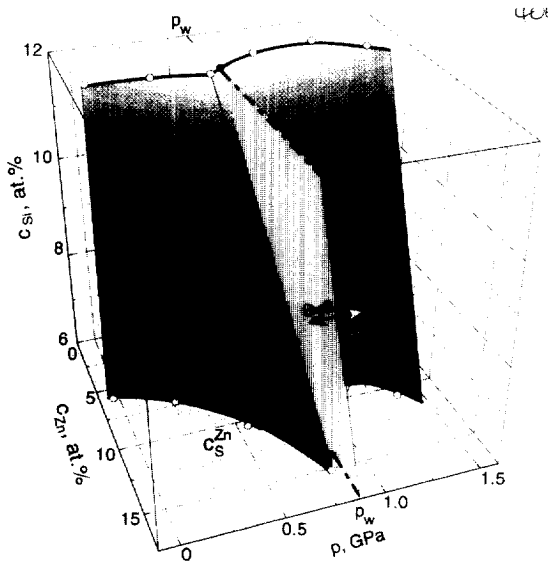

Fig. 7. Quasibinary three-dimensional bulk phase diagram for Fe–Si–Zn system in Zn concentration–Si concentration–pressure coordinates along with surface of wetting/dewetting phase transition (light) for the 38°⟨001⟩tilt GB.

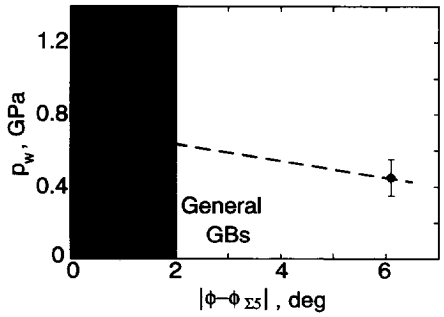

Fig. 8. Dependence of GB dewetting phase transition pressure p_w on deviation from Σ5 coincidence misorientation in ⟨001⟩ zone. The region of existence of the special Σ5 GB is filled with a dark colour.

chemical effects were to dominate, the $\theta(p)$ dependence would also be non-monotonic, following the pressure dependence of the solidus, which is not the case. Therefore, in a first rough approximation we will consider the excess volume as the only reason for the change in the interfacial energy under high pressure.

4.1. Estimation of the excess volume of the solid/liquid interface

The structural misfit at the GB and solid/liquid interfaces causes a lower density than in the bulk atomic packaging. The resulting excess volume or free volume has been studied using hard sphere and computer models of interfaces [2, 12]. However, until now the excess volume was not experimentally accessible, except for high resolution studies of the interface structure, in which the excess volume is a structural parameter. In the present work the excess volume can be accessed as a thermodynamic parameter. From equation (1) it follows that the $\theta(p)$ dependence takes the following form:

$$\theta = 2 \arccos\left\{\frac{\gamma^0_{GB} + p\Delta v_{GB}}{2(\gamma^0_{SL} + p\Delta v_{SL})}\right\} \qquad (3)$$

where γ^0_{GB} and γ^0_{SL} are the excess energies of the GB and solid/liquid interface at the fixed constant Zn concentration; Δv_{GB} and Δv_{SL} are the excess volumes of these interfaces, respectively. The experimental $\theta(p)$ dependencies have been fitted using equation (3) with the following values: $\gamma^0_{SL} = 0.3 \pm 0.1$ J/m^2, $\gamma^0_{GB} = 0.8 \pm 0.2$ J/m^2, and $\Delta v_{GB} = 0.6$ Å [2, 13, 14]. It follows from the fitting procedure that for all four boundaries studied, $\Delta v_{SL} = 2.5 \pm 1.5$ Å. This is a relatively large value compared to the excess volume expected for GBs, which is an indication that the structural misfit at the solid/liquid interface is larger than that at the GB. If we assume that the deficit of density in the core of the interfaces is the same for the GB and solid/liquid interface and accept 5 Å as the structural GB width, then the width of the solid/liquid interface is 20 ± 10 Å.

4.2. The nature of the excess volume

An important question is why $2\Delta v_{SL} > \Delta v_{GB}$, because the analysis of the atomic structure of the solid/liquid interface in pure metals predicts an interface excess volume close to 0 [12]. We think that the high value of the excess volume in our case is connected with the difference in the composition of the crystalline and liquid phases. Therefore, the structure of the solid/liquid interface should be considered on the atomic level, at least qualitatively. The complete wetting of GBs by a liquid or amorphous phase whose composition is different from that of the bulk phase is also commonly observed in ceramics. Since the work of Clarke and Thomas [15], where the presence of an approximately 1 nm wide amorphous film on GBs in MgO hot-pressed silicon nitride was observed, such films have been found in a number of ceramic materials, such as silicon nitride with different additives, zinc oxide varistor ceramics, certain silicon carbides, capacitor dielectrics, single-phase tetragonal and partially stabilized zirconia ceramics, nuclear waste ceramics and aluminas [9 ,16]. It was found that the thickness of the amorphous intergranular phase in such ceramics varies in a rather narrow interval around 1 nm. A detailed analysis of the stability of the thin intergranular glass phase in ceramics has been carried out by Clarke [17]. He supposed that the relative constancy of the glass film thickness implies that this is an equilibrium thickness value, which is determined by the competition of the long-range van der Waals *attraction* of two crystalline halves and the *repulsive* structural component of the disjoining pressure (see also Ref. [18], where the dependence of the equilibrium film thickness on the composition of the amorphous phase has been investigated). Generally, the structural component of the disjoining pressure arises due to the overlapping of the perturbations of the homogeneous liquid or amorphous phase induced by the crystalline grains. Clarke applied a mean field approach for the estimations where the degree of the crystal-induced order in the amorphous phase is described by a scalar order parameter, and the free energy density of the amorphous phase is given by the standard Landau–Ginsburg equation. It is known, however, that the accuracy of this approach drops as the gradient of the order parameter becomes comparable with the inverse interatomic distance. One can speculate that for the case of silica films the order parameter is determined by the orientation of the SiO_4 tetrahedra (silica molecules) which varies continuously at relatively large distances, and the Ginsburg–Landau theory can be applied; however, for our case of elementary metals the inverse gradient of the order parameter has the order of magnitude of the interatomic distance, and the mean field approximation fails. Therefore, in further considerations

we will restrict ourselves to a qualitative picture of the phenomenon.

For the description of the properties of liquid alloys the radial distribution function $G(r)$ is very useful [19]. It is determined by the probability density of finding two atoms at a distance r from each other. For a solid metal at 0 K, $G(r)$ can be represented by a set of δ-like peaks associated with the shells of nearest, next-nearest and higher order neighbours. These peaks broaden and shift to higher values of r (thermal expansion) as the temperature increases. For the melts of a close-packed metal $G(r)$ has maxima at distances that correspond to the few first coordination shells in the solid state, the amplitude of the maxima decreasing rapidly with the shell number. Wolf and Merkle [2] applied the description in terms of $G(r)$ to the GBs. Due to structural disorder at the GBs the peaks of $G(r)$ defined for the GB plane are already broadened and shifted from the positions determined by the ideal crystal toward higher r values at 0 K. Clarke's arguments can be reformulated in terms of the $G(r)$ function as follows: in the melted or amorphous phase near the solid/liquid interface owing to the influence of the crystalline phase, additional peaks in the $G(r)$ function should appear which correspond to the coordination shells in the crystal. In the same manner the atom positions in the crystal near the interface are influenced by the adjacent melt: additional peaks at positions characteristic of the melt appear in $G(r)$. The averaged interatomic distance is given by an expression of the type

$$\int r^3 G(r)\mathrm{d}r. \tag{4}$$

Therefore, if we take into account that the Zn atoms are larger than the Fe atoms (1.37 Å and 1.27 Å, respectively), the liquid Zn-rich alloy near the interface should be compressed and the solid Fe-based alloy expanded. The order parameter η from Clark's consideration can be introduced as a Fourier transform of $G(r)$ with the wave vector from the reciprocal lattice of a crystal. The schematic dependence of η on the distance z across two solid/liquid interfaces is shown in Fig. 9. The region of decreased order in the crystal near the interface is expanded and the adjacent regions of the melt with increased order (in comparison with the order of the melt far from the interface where $\eta = 0$) are compressed. The contribution of the crystal to the excess volume should be higher than that of the melt because the total excess volume is positive. The reason for this is the asymmetry of the interatomic potentials: decreasing the interatomic distance from equilibrium by some value always costs more energy than increasing the interatomic distance by the same value. In Fig. 9 the $\eta(z)$ dependence for a GB is shown. Both the computer simulations [20] and experimental observations [21] show that some degree of crystalline order remains in the GBs up to

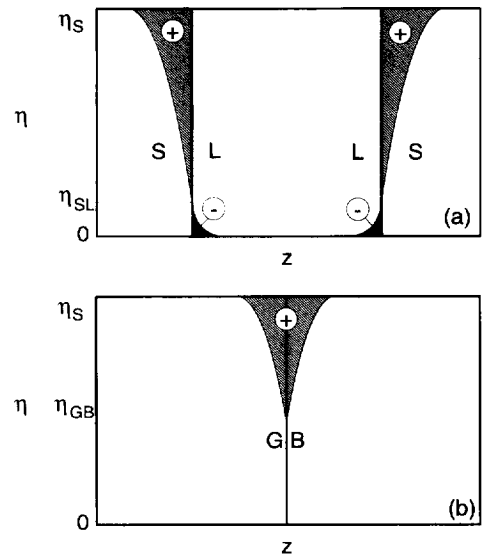

Fig. 9. Schematic dependence of crystalline order parameter η on distance z across the two solid (S)/liquid (L) interfaces (a) and across the GB (b). The hatched regions of the decreased order in the crystal are expanded (positive excess volume) and the regions of the non-zero order in the liquid near the interface (dark shaded areas) are compressed (negative excess volume). Note that in the GB, $\eta_{GB} > 0$; η_S and η_{SL} denote the order parameters in the bulk far from the interface and at the geometrical position of the solid/liquid interface, respectively.

temperatures very close to the melting point. Therefore, the crystal expansion in the GB is lower than twice the expansion at the solid/liquid interface, and the GB should be energetically favourable at high hydrostatic pressures.

4.3. *Misorientation effect on the wetting pressure*

Figure 8 shows that the dewetting phase transition pressure increases as the misorientation approaches the $\Sigma 5$ special boundary. From equations (2) and (3) one can get the following expression for the wetting/dewetting transition pressure:

$$p_w = \frac{\gamma_{GB} - 2\gamma_{SL}}{2\Delta v_{SL} - \Delta v_{GB}}. \tag{5}$$

The observed $p_w(\phi)$ dependence is completely incomprehensible if only equation (5) is considered, because it is generally believed that special GBs have a low value of the excess surface energy and excess volume and according to equation (5) this should lead to a minimum on the p_w misorientation dependence at the special misorientation, which is exactly opposite to the experimental situation. However, in concentrated alloys the characteristic cusps on the $\gamma_{GB}(\phi)$ dependencies at special misorientations may not occur. For instance, it was shown [22] that the difference in the mobility between special and general large-angle GBs has already disappeared at low levels of a segregating impurity in the alloy. The results of Wang *et al.* [3] also fail to demonstrate any energetic

cusps at special misorientations in the Ni–5 at.% Cu alloy at elevated temperatures. Therefore, the $p_w(\phi)$ dependence in our case can be determined by the misorientation dependence of γ_{SL} rather than γ_{GB}. Indeed, the (013) plane has the highest interplanar spacing after (001) in the family of planes forming symmetrical tilt ⟨001⟩ GBs [23]. The correlation between the interplanar spacing and interface energy is well known [2]. According to equation (5) the minimum in γ_{SL} at the special Σ5 misorientation leads to the maximum on the $p_w(\phi)$ dependence, which is actually observed in the experiment.

4.4. *Influence of the Si content*

The dewetting pressure p_w is lower for the alloy with 12 at.% Si than for the alloy with 6 at.% Si for the same 38°⟨001⟩ GB. This is not surprising since it has been shown [11] that the wetting phase transition of the 38°⟨001⟩ GB in Fe–12 at.% Si by the Zn-rich melt occurs at approx. 750°C (see also Fig. 6), while for Fe–5 at.% Si complete wetting of the GB by the melt has been observed down to the lowest temperature studied (660°C). For similar values of the excess entropies of the interfaces this means a lower value of the γ_{GB}–$2\gamma_{SL}$ difference for the Si-rich alloy at the constant temperature T_0 (see Fig. 10). Let us consider the problem quantitatively. The segregation of Si to the GBs in Fe–Si alloys is well established experimentally [24]. According to the Gibbs adsorption equation, an increase in the concentration (and chemical potential) of the segregating impurity in the bulk of the alloy leads to a decrease in the GB energy. However, as we have seen in the previous section, the behaviour of γ_{SL} is also very important in determining p_w. It is impossible to estimate the change in γ_{SL} caused by the increase in the Si concentration in the alloy based on the Gibbs adsorption equation, because no information on the adsorption at the solid/liquid interface is available. Moreover, the degree of adsorption depends on the arbitrary definition of the geometrical position of the interface. For estimations, we will use the division of the interfacial energy into chemical and physical parts which was first proposed by Meidema and den Broeder [14]. The chemical contribution arises from the different types of neighbourhood between the Fe, Si and Zn atoms across the interface and can be easily generalized to three-component systems starting from Turnbull's expression for binary systems [25] in the regular solution approximation:

$$\gamma_{SL}^{chem} = s\alpha_{SL}\Big[\Omega_{Fe\text{-}Zn}(c_L^{Zn} - c_S^{Zn})^2 + \Omega_{Fe\text{-}Si}(c_L^{Si} - c_S^{Si})^2 + (\Omega_{Fe\text{-}Zn} + \Omega_{Fe\text{-}Si} - \Omega_{Zn\text{-}Si})(c_L^{Zn} - c_S^{Zn})(c_L^{Si} - c_S^{Si})\Big] \quad (6)$$

where $\Omega_{Fe\text{-}Zn}$, $\Omega_{Fe\text{-}Si}$ and $\Omega_{Zn\text{-}Si}$ are the interaction parameters from the regular solution theory; α_{SL} is the fraction of the unbroken bonds at the solid/liquid interface; c_L^{Zn}, c_L^{Si} and c_S^{Si} are the liquidus Zn concentration, the liquidus Si concentration and the concentration of Si in the solid Fe–Zn–Si alloy, respectively; s is the number of atoms per unit area of interface. Meidema and den Broeder [14] estimated the value of γ_{SL}^{chem} for the binary Fe–Zn system to be approximately 100 mJ/m², which is a significant contribution to the total energy of about 300 mJ/m². Therefore, we think that the variation in the chemical part of the excess energy of the solid/liquid interface is decisive for small variations in the bulk composition. The parameter $\Omega_{Fe\text{-}Zn}$ can be estimated from the integral mixing enthalpy for a solid Fe–20 at.% Zn alloy at 793°C [26]: $\Omega_{Fe\text{-}Zn} \approx 12$ kJ/mol. From the data of Inden and Pitsch [27] $\Omega_{Fe\,Si} \approx -92$ kJ/mol. There are no reliable data on the thermodynamic parameters of Si–Zn alloys, but because of the negligible mutual solubility of Si and Zn [28] (which means that $c_L^{Si} \approx 0$ in our case) one can assume that $\Omega_{Zn\text{-}Si} > 0$. It follows then from equation (6) that γ_{SL}^{chem} increases at least by 25% of its absolute value as the c_S^{Si} increases from 6 to 12 at.%. According to equation (5), this increase contributes to the observed decrease in p_w, which is in agreement with the experimental data.

It should be noted that the dependence of γ_{SL} and γ_{GB} on the Zn concentration transforms equation (5) to a transcendental one with respect to p_w, because the Zn solidus concentration, at which γ_{SL} and γ_{GB} should be measured, is pressure dependent. It follows from our previous work [6] that the influence of the concentration changes on γ_{GB} is stronger than on γ_{SL}. This can be the reason why the pressure at which the maximum in the $c_S^{Zn}(p)$ dependence occurs is so close to p_w.

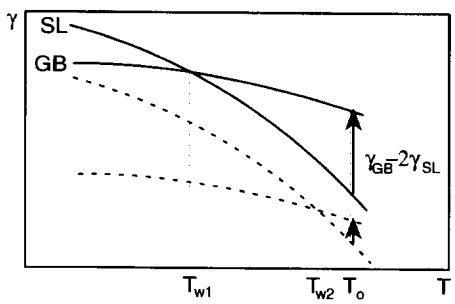

Fig. 10. Schematic temperature dependencies of excess free energies of GBs and doubled solid/liquid (SL) interfaces in Fe–6 at.% Si (solid line) and Fe–12 at.% Si (dashed line).

5. CONCLUSIONS

1. The transition from complete to incomplete wetting of high-angle ⟨001⟩ tilt GBs in Fe–Si alloys by a Zn-rich melt (dewetting phase transition) occurs

as the hydrostatic pressure increases. The dewetting phase transition pressure p_w at 905°C varies in the interval 0.4–0.9 GPa. The p_w value is higher for the special Σ5 GB than for general large-angle GBs and decreases with increase in the Si concentration in the alloy.

2. Three-dimensional phase diagrams in temperature–Zn concentration–pressure and Si concentration–Zn concentration–pressure coordinates have been plotted. In these diagrams the lines both for the bulk of the alloy and for the GB are presented.

3. The dewetting transition due to a pressure increase indicates that twice the excess volume of the solid/liquid interface is higher than the excess volume of all GBs studied. The estimated excess volume of the solid/liquid interface is 2.5 ± 1.5 Å. This large value is explained in terms of the relatively thick solid/liquid interface and a large structural misfit.

4. The nature of the excess volume of the solid/liquid interface has been discussed. Its high absolute value is most probably due to a large difference in the size of the Fe and Zn atoms and the asymmetry of the interatomic potentials.

5. It is suggested that the reason for the observed misorientation dependence of p_w is the anisotropy of the solid/liquid interfacial energy. The dependence of p_w on the Si concentration in ternary Fe–Si–Zn alloys has been analysed in the framework of the regular solution approximation. The increase in the energy of the solid/liquid interface with increasing Si content in the solid contributes to the observed decrease in p_w.

Acknowledgements—The authors are grateful to Professor R. A. Fournelle and Dr V. N. Semenov for fruitful discussions. Professor M. Rühle is gratefully acknowledged for his interest in this work and for reading the manuscript. This work was partly supported by the Volkswagen Foundation under contract I/69 000 and the Polish Committee for Scientific Research under contract 3 p407 008 04.

REFERENCES

1. Keene, B. J., *Int. Mater. Rev.*, 1993, **38,** 157.
2. Wolf, D. and Merkle, K. L., in *Materials Interfaces*, ed. D. Wolf and S. Yip. Chapman & Hall, London, 1992, p. 87.
3. Wang, H. Y., Najafabadi, R., Srolovitz, D. J. and Lesar, R., *Acta. metall. mater.*, 1993, **41,** 2533.
4. Straumal, B., Gust, W. and Molodov, D., *J. Phase Equilibria*, 1994, **15,** 386.
5. Straumal, B., Muschik, T., Gust, W. and Predel, B., *Acta metall. mater.*, 1992, **40,** 939.
6. Rabkin, E. I., Gust, W., Łojkowski, W. and Paidar, V., *Interface Sci.*, 1993, **1,** 201.
7. Straumal, B. B. and Shvindlerman, L. S., *Acta metall.*, 1985, **33,** 1735.
8. Cheng, V. M., Allen, P. C. and Lazarus, D., *Appl. Phys. Lett.*, 1975, **26,** 6.
9. Clarke, D. R. and Gee, M. L., in *Materials Interfaces*, ed. D. Wolf and S. Yip. Chapman & Hall, London, 1992, p. 255.
10. Rabkin, E. I., Semenov, V. N., Shvindlerman, L. S. and Straumal, B. B., *Acta metall. mater.*, 1991, **39,** 627.
11. Noskovich, O. I., Rabkin, E. I., Semenov, V. N., Straumal, B. B. and Shvindlerman, L. S., *Acta metall. mater.*, 1991, **39,** 3091.
12. Spaepen, F., *Acta metall.*, 1975, **23,** 729.
13. Missol, W., *Energies of Interfaces in Metals*. Slask, Katowice, 1975.
14. Miedema, A. R. and den Broeder, F. J. A., *Z. Metallk.*, 1979, **70,** 14.
15. Clarke, D. R. and Thomas, G., *J. Am. Ceram. Soc.*, 1977, **60,** 491.
16. Cinibulk, M. K., Kleebe, H.-J., Schneider, G. A. and Rühle, M., *J. Am. Ceram. Soc.*, 1993, **76,** 2801.
17. Clarke, D. R., *J. Am. Ceram. Soc.*, 1987, **70,** 15.
18. Tanaka, I., Kleebe, H.-J., Cinibulk, M. K., Bruley, J., Clarke, D. R. and Rühle, M., *J. Am. Ceram. Soc.*, 1994, **77,** 911.
19. Isihara, A., *Statistical Physics*. Academic Press, New York, 1971, p. 165.
20. Lutsko, J. F., Wolf, D., Phillpot, S. R. and Yip, S., *Phys. Rev. B*, 1989, **40,** 2841.
21. Hsieh, T. E. and Balluffi, R. W., *Acta metall.*, 1989, **37,** 1637.
22. Fridman, E. M., Kopezky, Ch. V. and Shvindlerman, L. S., *Z. Metallk.*, 1975, **66,** 533.
23. Paidar, V., *Acta metall.*, 1987, **35,** 2035.
24. Lejček and Hofmann, S., *Interface Sci.*, 1993, **1,** 163.
25. Turnbull, D., in *Impurities and Imperfections*. Amer. Soc. Metals, Metals Park, Ohio, 1955, p. 121.
26. Hultgren, R. *et al.*, *Selected Values of the Thermodynamic Properties of Binary Alloys*. Amer. Soc. Metals, Metals Park, Ohio, 1973, pp. 878, 906.
27. Inden, G. and Pitsch, W., *Z. Metallk.*, 1971, **62,** 627.
28. Massalski, T. B. *et al.* (ed.), *Binary Alloy Phase Diagrams*. ASM International, Materials Park, Ohio, 1990, 1993.